

15. Soref, R. A. & Lorenzo, J. P. Light-by-light modulation in silicon-on-insulator waveguides. *Digest of the OSA Integrated and Guided-Wave Optics Topical Meeting* 86–89 (Optical Society of America, Washington DC, 1989).

16. Barrios, C. A., Almeida, V. R. & Lipson, M. Low-power-consumption short-length and high-modulation-depth silicon electrooptic modulator. *J. Lightwave Technol.* **21**, 1089–1098 (2003).

17. Soref, R. A. & Bennett, B. R. Kramers-Kronig analysis of electro-optical switching in silicon. *Proc. SPIE* **704**, 32–37 (1987).

18. Zhao, C. Z., Li, G. Z., Liu, E. K., Gao, Y. & Liu, X. D. Silicon on insulator Mach–Zehnder waveguide interferometers operating at 1.3 μm . *Appl. Phys. Lett.* **67**, 2448–2449 (1995).

19. Stepanov, S. & Ruschin, S. Modulation of light by light in silicon-on-insulator waveguides. *Appl. Phys. Lett.* **83**, 5151–5153 (2003).

20. Liu, A. *et al.* A high-speed silicon optical modulator based on a metal-oxide-semiconductor capacitor. *Nature* **427**, 615–618 (2004).

21. Almeida, V. R., Panepucci, R. R. & Lipson, M. Nanotaper for compact mode conversion. *Opt. Lett.* **28**, 1302–1304 (2003).

22. Verdeyen, J. T. *Laser Electronics*, 3rd edn 153 (Prentice Hall, Upper Saddle River, NJ, 2000).

23. Chin, A., Lee, K. Y., Lin, B. C. & Horng, S. Picosecond photoresponse of carriers in Si ion-implanted Si. *Appl. Phys. Lett.* **69**, 653–655 (1996).

24. Meindl, J. D. *et al.* Interconnect opportunities for gigascale integration. *IBM Res. Dev.* **46**, 245–263 (2002).

25. Weiss, S. M., Molinari, M. & Fauchet, P. M. Temperature stability for silicon-based photonic band-gap structures. *Appl. Phys. Lett.* **83**, 1980–1982 (2003).

26. Cheben, P., Xu, D.-X., Janz, S. & Delage, A. Scaling down photonic waveguide devices on the SOI platform. *Proc. SPIE* **5117**, 147–156 (2003).

27. Vlasov, Y. A. & McNab, S. J. Losses in single-mode silicon-on-insulator strip waveguides and bends. *Opt. Express* **12**, 1622–1631 (2004).

28. Pardo, F. *et al.* Optical MEMS devices for telecom systems. *Proc. SPIE* **5116**, 435–444 (2003).

29. Miller, D. A. B. Optical interconnects to silicon. *IEEE J. Sel. Top. Quant. Electron.* **6**, 1312–1317 (2000).

Acknowledgements We acknowledge support by the Cornell Center for Nanoscale Systems, funded by the National Science Foundation (NSF), by the Air Force Office of Scientific Research (AFOSR) and by the CS-WDM programme of the Defense Advanced Research Project Agency. V.R.A. acknowledges sponsorship support provided by the Brazilian Defence Ministry. This work was performed in part at the Cornell Nano-Scale Science & Technology Facility (CNF), a member of the National Nanotechnology Infrastructure Network (NNIN) which is supported by the NSF, its users, Cornell University and Industrial Affiliates.

Competing interests statement The authors declare that they have no competing financial interests.

Correspondence and requests for materials should be addressed to M.L. (lipson@ece.cornell.edu).

Unusual activity of the Sun during recent decades compared to the previous 11,000 years

S. K. Solanki¹, I. G. Usoskin², B. Kromer³, M. Schüssler¹ & J. Beer⁴

¹Max-Planck-Institut für Sonnensystemforschung (formerly the Max-Planck-Institut für Aeronomie), 37191 Katlenburg-Lindau, Germany

²Sodankylä Geophysical Observatory (Oulu unit), University of Oulu, 90014 Oulu, Finland

³Heidelberger Akademie der Wissenschaften, Institut für Umweltphysik, Neuenheimer Feld 229, 69120 Heidelberg, Germany

⁴Department of Surface Waters, EAWAG, 8600 Dübendorf, Switzerland

Direct observations of sunspot numbers are available for the past four centuries^{1,2}, but longer time series are required, for example, for the identification of a possible solar influence on climate and for testing models of the solar dynamo. Here we report a reconstruction of the sunspot number covering the past 11,400 years, based on dendrochronologically dated radiocarbon concentrations. We combine physics-based models for each of the processes connecting the radiocarbon concentration with sunspot number. According to our reconstruction, the level of solar activity during the past 70 years is exceptional, and the previous period of equally high activity occurred more than 8,000 years ago. We find that during the past 11,400 years the Sun spent only of the order of 10% of the time at a similarly high level of

magnetic activity and almost all of the earlier high-activity periods were shorter than the present episode. Although the rarity of the current episode of high average sunspot numbers may indicate that the Sun has contributed to the unusual climate change during the twentieth century, we point out that solar variability is unlikely to have been the dominant cause of the strong warming during the past three decades³.

Sunspots—strong concentrations of magnetic flux at the solar surface—are the longest-studied direct tracers of solar activity. Regular telescopic observations are available after AD 1610. In addition to the roughly 11-year solar cycle, the number of sunspots, formalized in the group sunspot number¹ (GSN), exhibits prominent fluctuations on longer timescales. Notable are an extended period in the seventeenth century called the Maunder minimum, during which practically no sunspots were present², and the period of high solar activity since about AD 1940 with average sunspot numbers above 70.

A physical approach to reconstruction of the sunspot number back in time is based on archival proxies, such as the concentration of the cosmogenic isotopes ¹⁴C in tree rings^{4–6} or ¹⁰Be in ice cores^{7,8}. This approach has recently been strengthened by the development of physics-based models describing each link in the chain of processes connecting the concentration of cosmogenic isotopes with the sunspot number^{9–12}. This advance allowed a reconstruction of the sunspot number since AD 850 based on ¹⁰Be records from Antarctica and Greenland^{13,14}. The current period of high solar activity is unique within this interval, but the covered time span is too short to judge just how unusual the current state of solar activity is.

Here we present a reconstruction of the sunspot number covering the Holocene epoch, the modern period of relatively warm climate that superseded the glacial period about 11,000 years ago. The reconstruction is based on $\Delta^{14}\text{C}$, the ¹⁴C activity in the atmosphere¹⁵ obtained from high-precision ¹⁴C analyses on decadal samples of mid-latitude tree-ring chronologies. The data set has been created in an international collaboration of dendrochronolo-

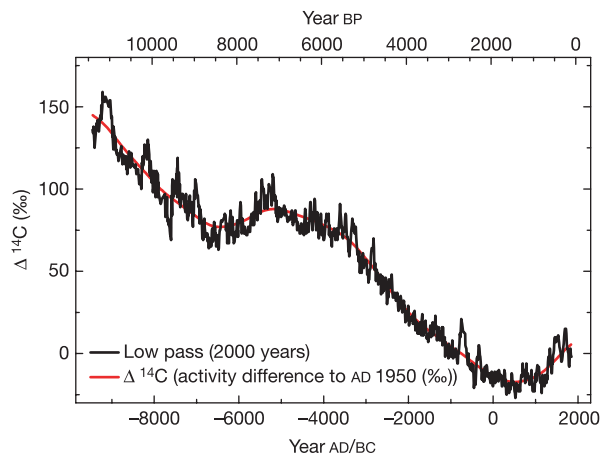


Figure 1 Atmospheric radiocarbon level $\Delta^{14}\text{C}$ (expressed as deviation, in ‰, from the AD 1950 standard level¹⁵) derived from mostly decadal samples of absolutely dated tree-ring chronologies (INTCAL98 data set)¹⁶. The $\Delta^{14}\text{C}$ measurement precision is generally 2–3‰, although in the earlier part of the time series it can reach up to 4–5‰. The INTCAL98 data for times earlier than 11,400 BP are not directly employed for the reconstruction because of larger errors and uncertainties in the carbon cycle acting at that time. See Supplementary Information for more information on the data set, initial conditions used for the reconstruction, and error estimates. The long-term decline (indicated by the red curve) is caused by a reduction in ¹⁴C production rate due mainly to an increase in the geomagnetic shielding of the cosmic ray flux. The short-term fluctuations (duration one to two centuries) reflect changes of the production rate due to solar variability. Years BC are shown negative here and in other figures.

gists and radiocarbon laboratories¹⁶. The absolutely and precisely dated original data set used for the sunspot number reconstruction is represented by the black line in Fig. 1. Starting at a level 15% higher than the reference level of AD 1950, the atmospheric ¹⁴C shows a long-term trend (indicated by the red line), which is mainly the result of changes in the intensity of the geomagnetic dipole field before and during the Holocene epoch. The fluctuations on shorter timescales predominantly result from variations of the ¹⁴C production rate due to heliomagnetic variability, which modulates the cosmic ray flux.

The atmospheric ¹⁴C level may also be affected by changes in the partition of carbon between the major reservoirs, that is, deep ocean, ocean mixed layer, biosphere and atmosphere. Variations in ocean circulation¹⁷ could influence ¹⁴C via a variable uptake of CO₂ into the ocean or by the exchange of ¹⁴C-depleted carbon from the deep ocean, but, owing to the rather small ¹⁴C gradients among the reservoirs, strong changes in these processes need to be invoked. For the Holocene, there is no evidence of considerable oceanic variability, so we can assume that the short- and mid-term fluctuations of ¹⁴C predominantly reflect solar variability. This is supported by the strong similarity of the fluctuations of ¹⁰Be in polar ice cores compared to ¹⁴C, despite their completely different geochemical history^{18–20}.

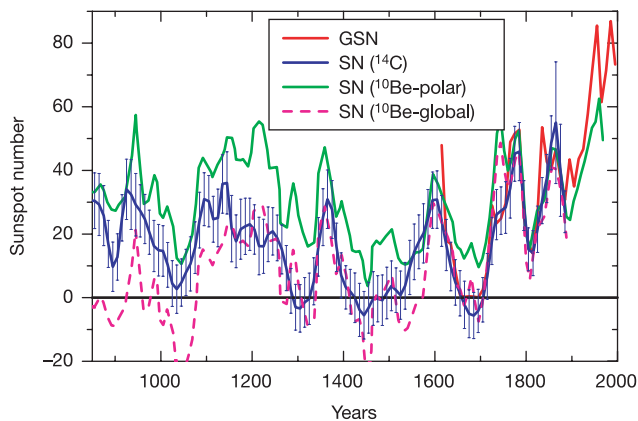


Figure 2 Comparison between directly measured sunspot number (SN) and SN reconstructed from different cosmogenic isotopes. Plotted are SN reconstructed from ^Δ¹⁴C (blue), the 10-year averaged group sunspot number¹ (GSN, red) since 1610 and the SN reconstruction¹⁴ from ¹⁰Be under the two extreme assumptions of local (green) and global (magenta, dashed) production, respectively. The slightly negative values of the reconstructed SN during the grand minima are an artefact; they are compatible with SN = 0 within the uncertainty of these reconstructions as indicated by the error bars. ^Δ¹⁴C is connected with the ¹⁴C production rate via a carbon cycle model²¹. The connection between the ¹⁴C production rate, *R*, and the cosmic ray flux is given by $R = \int_{\theta=0}^{\pi} \int_{P_c(\theta, M)}^{\infty} X(P, \Phi) Y(P) dP \sin \theta d\theta$, where θ is the colatitude relative to the geomagnetic dipole axis, and $P_c(\theta, M)$ is the local cosmic ray rigidity cutoff (which depends on θ and the virtual geomagnetic dipole moment, *M*)²³. $X(P, \Phi)$ is the differential cosmic ray rigidity spectrum near Earth, Φ is the modulation strength describing the average rigidity losses of cosmic rays inside the heliosphere, $Y(P)$ is the differential yield function²⁴ of ¹⁴C, and *P* is the rigidity of the primary cosmic rays. For studies of long-term changes of the cosmic ray flux, the parameter Φ alone adequately describes the modulation of the cosmic ray spectrum $X(P)$ ^{11,24}. The two most abundant cosmic ray species, protons and α -particles, are taken into account in the model¹³. The cosmic ray transport model relates *R* to Φ , which in turn depends on the Sun's open magnetic flux¹². The open flux is linked with the magnetic flux in sunspots (and thus with the SN) via the source term in a system of differential equations^{9,10}. The value of *R* is obtained from ^Δ¹⁴C and *M* is known for the whole interval of interest^{25,26}, so that Φ can be obtained from the inversion of the equation given above. Error bars depict the 68% confidence interval for the reconstructed SN, which takes into account both random and systematic uncertainties (see Supplementary Information).

We first determine the ¹⁴C production rate in the Earth's atmosphere following Usoskin and Kromer²¹. They used two distinct methods, which take into account carbon cycle effects in different ways. Both methods give similar results when applied to the tree-ring ^Δ¹⁴C data set described above. For the current reconstruction we use the average of the ¹⁴C production rate deduced using both techniques. In accordance with the decadal

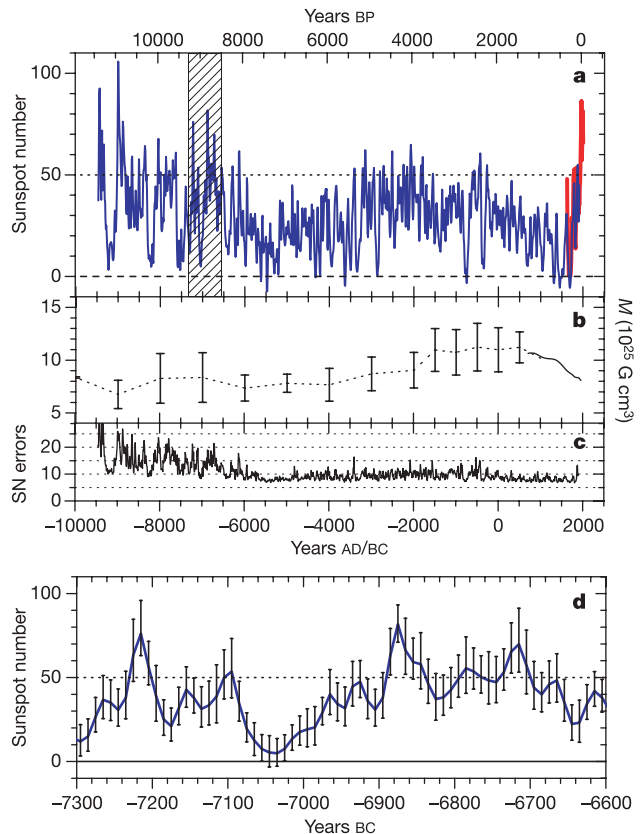


Figure 3 Reconstructed sunspot number and its uncertainty for the whole interval of time considered. **a**, 10-year averaged SN reconstructed from ^Δ¹⁴C data since 9500 bc (blue curve) and 10-year averaged group sunspot number¹ (GSN) obtained from telescopic observations since 1610 (red curve). The horizontal dotted line marks the threshold above which we consider the Sun to be exceptionally active. It corresponds to 1.3 standard deviations above the mean. **b**, Evolution of the virtual geomagnetic dipole moment²⁶ with error bars that take into account the scatter between different palaeomagnetic reconstructions. (The error bars give the s.d. in the reconstructed virtual geomagnetic dipole moment.) The geomagnetic field data of ref. 25 are given by the dotted line. **c**, Uncertainty in the reconstructed SN. It includes errors introduced at each step of the reconstruction process. The largest sources of random errors are the uncertainty in the knowledge of the geomagnetic dipole moment and in the ¹⁴C production rate. We also consider systematic errors—for example, due to uncertainties in the ¹⁴C production rate prior to the considered period of time. A discussion of how these uncertainties are estimated is given in Supplementary Information. Clearly, the uncertainties are sufficiently small that they do not affect the presence or absence of grand minima or of episodes of high activity, except in already marginal cases. **d**, A detail from the full time series of reconstructed SN with expanded temporal scale. The chosen interval (corresponding to the shaded part of **a**) exhibits three episodes of high solar activity and a grand minimum. The error bars indicate the total uncertainty, σ , in the reconstruction. (They depict the 68% confidence interval for the reconstructed SN, which takes into account both random and systematic uncertainties (see Supplementary Information).) The two strongest maxima lie 2.1 σ and 3.0 σ , respectively, above the high-activity threshold of 50. Hence the probability that they are due to statistical fluctuations related to these errors is 3% and 0.2%, respectively. The probability that a whole episode of high activity (lasting, say, 50 years) is due to a statistical fluctuation is significantly smaller.

sampling of the ^{14}C data we reconstruct the 10-year averaged sunspot number. Because the $\Delta^{14}\text{C}$ data are contaminated by extensive burning of ^{14}C -free fossil fuel since the late nineteenth century²² and later by atmospheric nuclear bomb tests, we use ^{14}C data before AD 1900 only and take the historical sunspot number record for the most recent period.

From the ^{14}C production rate we obtain the sunspot number in multiple steps, each substantiated by a physics-based model. A model describing the transport and modulation of galactic cosmic rays within the heliosphere¹¹ is inverted to find the cosmic ray flux corresponding to the determined ^{14}C production rate. The transport of galactic cosmic rays in the heliosphere is affected by the Sun's open magnetic flux, that is, the fraction of the Sun's total magnetic flux that reaches out into interplanetary space¹². The open flux is linked with the sunspot number by inverting a model describing the evolution of the open magnetic flux for given sunspot number^{9,10}. All adjustable parameters entering this chain of models

were fixed using independent data prior to the current reconstruction, so that no free parameter remains when reconstructing the sunspot number from ^{14}C data (see Supplementary Table S1). This reconstruction method was previously applied to ^{10}Be data from Greenland and Antarctica. Only the first step changes when using $\Delta^{14}\text{C}$ instead of ^{10}Be data to reconstruct the sunspot number. Hence, possible errors and uncertainties in the later steps are similar to those studied in our earlier papers^{13,14}.

Applying our reconstruction method to $\Delta^{14}\text{C}$, we first determine the sunspot number since AD 850 in order to compare these values with the historical record of GSNs since 1610 and with the reconstruction on the basis of ^{10}Be data¹⁴. Figure 2 shows that the reconstructed average sunspot number from $\Delta^{14}\text{C}$ is remarkably similar to the 10-year averaged GSN series (correlation coefficient $0.925_{-0.03}^{+0.02}$ with a false alarm probability $<10^{-6}$). The difference between the reconstructed and measured sunspot number is nearly gaussian with a standard deviation of 5.8, which is smaller than the theoretical estimate of the reconstructed sunspot number uncertainty (about 8 for the last millennium, see Supplementary Information), indicating the conservative nature of the latter. Two ^{10}Be -based sunspot number reconstructions are plotted in Fig. 2, which correspond to extreme assumptions about the geographic area of ^{10}Be production relevant for its deposition in polar ice. The local polar production model (green curve) provides an upper limit to the sunspot number¹⁴, while the global production model (magenta dashed curve) gives a lower limit¹³. The sunspot number time series obtained from $\Delta^{14}\text{C}$ lies between the two ^{10}Be -based reconstructions, and for the period after AD 1200 is closer to the ^{10}Be -based reconstruction under the assumption of global production.

Figure 3a shows the reconstruction based on the 11,400-year set of $\Delta^{14}\text{C}$ data. Clearly, the level of activity has remained variable, with episodes of particularly low numbers of sunspots (grand minima) distributed over the whole record. Episodes of high activity are also present. These are mostly concentrated in the earliest three millennia (before 6000 BC), which also exhibit a high average sunspot number (35.6 compared to 25.6 after 6000 BC). During the last eight millennia, the episode with the highest average sunspot number is the ongoing one that started about 60 years ago. The sunspot number averaged over the whole period is 28.7 with a standard deviation of 16.2. The average number of 75 since 1940 thus lies 2.85 standard deviations above this long-term average.

A major uncertainty in the reconstructed sunspot number is related to the evolution of the geomagnetic field, which is represented in Fig. 3b. A weaker geomagnetic field leads to an increased cosmic ray flux impinging on the terrestrial atmosphere and thus to a higher ^{14}C production rate, mimicking a lower value of sunspot number if not properly taken into account. The uncertainties in the reconstructed sunspot numbers are discussed in Supplementary Information and enter into Fig. 3c, where the sum of the random and systematic uncertainties affecting the reconstruction is given. For the whole time interval, the mean uncertainty of the reconstructed sunspot number is about 10.

In Fig. 3d we show a sub-interval of 700 years duration from our reconstruction, which exhibits three prominent periods of high sunspot number (average values exceeding 50) and a grand minimum. Within the 95% confidence interval, the Sun spent in total between 780 and 1,060 years in a high-activity state (sunspot number >50), which corresponds to 6.9–9.3% of the total duration of our reconstruction. The most probable values are 950 years and 8.3%, respectively. Although the rarity of the current episode of high average sunspot number may be taken as an indication that the Sun has contributed to the unusual degree of climate change during the twentieth century, we stress that solar variability is unlikely to be the prime cause of the strong warming during the last three decades³. In ref. 3, reconstructions of solar total and spectral irradiance as well as of cosmic ray flux were compared with surface temperature records

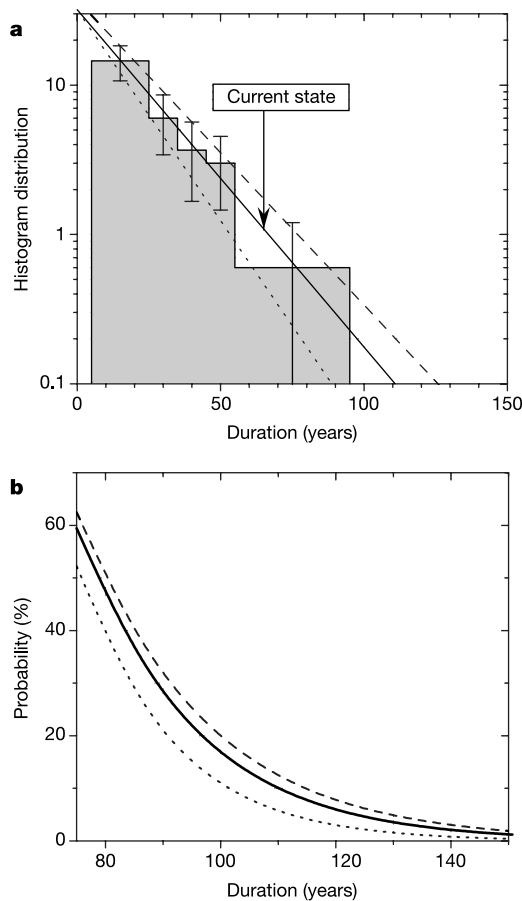


Figure 4 Distribution of the duration of episodes of high solar activity and the probability that the current episode will reach a given duration. **a**, Histogram of the distribution function of the duration of episodes of high solar activity during which the 10-year averaged SN exceeds 50. Some bins have been enlarged in order to improve the statistics; in such cases the average number per bin is given. The vertical error bars correspond to \sqrt{N} , where N is the number of events combined in one data point. The length of the current period of high activity is marked by the arrow. The solid line is a least-squares exponential fit to the plotted points. The dashed and dotted lines represent exponential fits to the distributions obtained from extreme SN reconstructions including the influence of random and systematic errors as given in Fig. 3 (see also the discussion in Supplementary Information). **b**, The probability of the total duration of a state of high activity (SN level exceeding 50). For the current episode, which started in AD 1940 (~ 65 years ago), the start of the diagram corresponds to the year AD 2015. Each curve is based upon the corresponding fit shown in **a**. The probability (for the reference curve) that the high activity continues for another 5 decades for a total duration of 115 years is only 8%.

covering approximately 150 years. It was shown that even under the extreme assumption that the Sun was responsible for all the global warming prior to 1970, at the most 30% of the strong warming since then can be of solar origin.

There are 31 periods during which the 10-year averaged sunspot number consistently exceeds a level of 50. The average length of such episodes is about 30 years, the longest being 90 years (around 9000 BC). The distribution of the durations of such episodes is given in Fig. 4a. The number of high-activity periods decreases exponentially with increasing duration. The current level of high solar activity has now already lasted close to 65 years and is marked by the arrow on the figure. This implies that not only is the current state of solar activity unusually high, but also this high level of activity has lasted unusually long. Assuming the previous episodes of high activity to be typical, we can estimate the probability with which the solar activity level will remain above a sunspot number of 50 over the next decades. The result is given in Fig. 4b, which shows that there is only a probability of $8\%_{-4\%}^{+3\%}$ that the current high-activity episode will last another 50 years (and thus reach a total duration of 115 years), while the probability that it will continue until the end of the twenty-first century is below 1%. □

Received 20 February; accepted 1 September 2004; doi:10.1038/nature02995.

- Hoyt, D. V. & Schatten, K. H. Group sunspot numbers: A new solar activity reconstruction. *Sol. Phys.* **179**, 189–219 (1998).
- Eddy, J. A. The Maunder minimum. *Science* **192**, 1189–1202 (1976).
- Solanki, S. K. & Krivova, N. Can solar variability explain global warming since 1970? *J. Geophys. Res.* **108**, doi: 10.1029/2002JA009753 (2003).
- Stuiver, M. & Braziunas, T. F. Atmospheric ^{14}C and century-scale solar oscillations. *Nature* **338**, 405–408 (1989).
- Stuiver, M. & Braziunas, T. F. Sun, ocean, climate and atmospheric $^{14}\text{CO}_2$: an evaluation of causal and spectral relationships. *Holocene* **3**, 289–305 (1993).
- Damon, P. E. & Sonett, C. P. in *The Sun in Time* (eds Sonnet, C. P., Giampapa, M. S. & Matthews, M. S.) 360–388 (Univ. Arizona, Tucson, 1991).
- Beer, J. *et al.* Use of ^{10}Be in polar ice to trace the 11-year cycle of solar activity. *Nature* **347**, 164–166 (1990).
- Beer, J. Long-term indirect indices of solar variability. *Space Sci. Rev.* **94**, 53–66 (2000).
- Solanki, S. K., Schüssler, M. & Flügge, M. Evolution of the Sun's large-scale magnetic field since the Maunder minimum. *Nature* **408**, 445–447 (2000).
- Solanki, S. K., Schüssler, M. & Flügge, M. Secular variation of the Sun's magnetic flux. *Astron. Astrophys.* **383**, 706–712 (2002).
- Usoskin, I. G., Alanko, K., Mursula, K. & Kovaltsov, G. A. Heliospheric modulation strength during the neutron monitor era. *Sol. Phys.* **207**, 389–399 (2002).
- Usoskin, I. G., Mursula, K., Solanki, S. K., Schüssler, M. & Kovaltsov, G. A. A physical reconstruction of cosmic ray intensity since 1610. *J. Geophys. Res.* **107**, doi:10.1029/2002JA009343 (2002).
- Usoskin, I. G., Mursula, K., Solanki, S. K., Schüssler, M. & Alanko, K. Reconstruction of solar activity for the last millennium using ^{10}Be data. *Astron. Astrophys.* **413**, 745–751 (2004).
- Usoskin, I. G., Solanki, S. K., Schüssler, M., Mursula, K. & Alanko, K. A millennium scale sunspot number reconstruction: evidence for an unusually active Sun since the 1940s. *Phys. Rev. Lett.* **91**, 211101 (2003).
- Stuiver, M. & Pollach, P. Discussion: reporting of ^{14}C data. *Radiocarbon* **19**, 355–363 (1977).
- Stuiver, M. *et al.* INTCAL98 Radiocarbon age calibration. *Radiocarbon* **40**, 1041–1083 (1998).
- Broecker, W. S. An unstable superconveyor. *Nature* **367**, 414–415 (1994).
- Bond, G. *et al.* Persistent solar influence on North Atlantic surface circulation during the Holocene. *Science* **294**, 2130–2136 (2001).
- Muscheler, R., Beer, J. & Kromer, B. *Solar Variability as an Input to the Earth's Environment* 305–316 (ESA SP-535, European Space Agency, Noordwijk, 2003).
- Bard, E., Raisbeck, G. M., Yiou, F. & Jouzel, J. Solar modulation of cosmogenic nuclide production over the last millennium: comparison between ^{14}C and ^{10}Be records. *Earth Planet. Sci. Lett.* **150**, 453–462 (1997).
- Usoskin, I. G. & Kromer, B. Reconstruction of the ^{14}C production rate from measured relative abundance. *Radiocarbon* (in the press).
- Suess, H. E. Radiocarbon content in modern wood. *Science* **122**, 415–417 (1955).
- Elsasser, W., Ney, E. P. & Winckler, J. R. Cosmic-ray intensity and geomagnetism. *Nature* **178**, 1226–1227 (1956).
- Castagnoli, G. & Lal, D. Solar modulation effects in terrestrial production of carbon-14. *Radiocarbon* **22**, 133–158 (1980).
- Hongre, L., Hulot, G. & Khokhlov, A. An analysis of the geomagnetic field over the past 2000 years. *Phys. Earth Planet. Inter.* **106**, 311–335 (1998).
- Yang, S., Odah, H. & Shaw, J. Variations in the geomagnetic dipole moment over the last 12000 years. *Geophys. J. Int.* **140**, 158–162 (2000).

Supplementary Information accompanies the paper on www.nature.com/nature.

Competing interests statement The authors declare that they have no competing financial interests.

Correspondence and requests for materials should be addressed to S.K.S. (solanki@mps.mpg.de).

Archaeology and age of a new hominin from Flores in eastern Indonesia

M. J. Morwood¹, R. P. Soejono², R. G. Roberts³, T. Sutikna², C. S. M. Turney³, K. E. Westaway³, W. J. Rink⁴, J.-x. Zhao⁵, G. D. van den Bergh⁶, Rokus Awe Due², D. R. Hobbs¹, M. W. Moore¹, M. I. Bird⁷ & L. K. Fifield⁸

¹Archaeology and Palaeoanthropology, School of Human and Environmental Studies, University of New England, Armidale, New South Wales 2351, Australia
²Indonesian Centre for Archaeology, Jl. Raya Condet Pejaten No. 4, Jakarta 12001, Indonesia

³GeoQuEST Research Centre, School of Earth and Environmental Sciences, University of Wollongong, Wollongong, New South Wales 2522, Australia

⁴School of Geography and Geology, McMaster University, Hamilton, Ontario L8S 4K1, Canada

⁵Advanced Centre for Queensland University Isotope Research Excellence (ACQUIRE), University of Queensland, Brisbane, Queensland 4072, Australia

⁶Royal Netherlands Institute for Sea Research, 1790 AB Den Burg, Texel, The Netherlands

⁷School of Geography and Geosciences, University of St Andrews, St Andrews, Fife KY16 9AL, UK

⁸Research School of Physical Sciences and Engineering, Australian National University, Canberra, ACT 0200, Australia

Excavations at Liang Bua, a large limestone cave on the island of Flores in eastern Indonesia, have yielded evidence for a population of tiny hominins, sufficiently distinct anatomically to be assigned to a new species, *Homo floresiensis*¹. The finds comprise the cranial and some post-cranial remains of one individual, as well as a premolar from another individual in older deposits. Here we describe their context, implications and the remaining archaeological uncertainties. Dating by radiocarbon (^{14}C), luminescence, uranium-series and electron spin resonance (ESR) methods indicates that *H. floresiensis* existed from before 38,000 years ago (kyr) until at least 18 kyr. Associated deposits contain stone artefacts and animal remains, including Komodo dragon and an endemic, dwarfed species of *Stegodon*. *H. floresiensis* originated from an early dispersal of *Homo erectus* (including specimens referred to as *Homo ergaster* and *Homo georgicus*)¹ that reached Flores, and then survived on this island refuge until relatively recently. It overlapped significantly in time with *Homo sapiens* in the region^{2,3}, but we do not know if or how the two species interacted.

Liang Bua is a cave formed in Miocene limestone on Flores, an island in eastern Indonesia located midway between the Asian and Australian continents (Fig. 1). The cave is situated 14 km north of Ruteng and 25 km from the north coast, overlooking the Wae Racang river valley at an altitude of 500 m above sea level (08° 31' 50.4" S, 120° 26' 36.9" E). It is 30 m wide and 25 m high at the entrance, and up to 40 m deep (Fig. 2). Formed as an underground cavern by karst dissolution, the northern end was then exposed by invasion of the Wae Racang. This river now lies 200 m distant from and 30 m below Liang Bua, but five river terraces at different elevations in the valley indicate a complex process of incision over a substantial period.

Our research at Liang Bua aims to recover evidence for the history of hominin evolution, dispersal and cultural and environmental change on Flores—an island with evidence of Early Pleistocene hominin occupation by 840 kyr^{4,5}. Work involved removing backfill from four previously excavated Sectors (I, III, IV and VII) and then continuing the excavations. We have reached a maximum depth of 11 m without encountering bedrock.